

# Constraints on neutrino non-standard interactions from COHERENT and PandaX-4T

Gang Li,<sup>2,\*</sup> Chuan-Qiang Song,<sup>1,3,4,†</sup> Feng-Jie Tang,<sup>1,3,4,‡</sup> and Jiang-Hao Yu<sup>1,3,4,5,§</sup>

<sup>1</sup>*School of Fundamental Physics and Mathematical Sciences, Hangzhou  
Institute for Advanced Study, UCAS, Hangzhou 310024, China*

<sup>2</sup>*School of Physics and Astronomy, Sun Yat-sen University, Zhuhai 519082, P.R. China*

<sup>3</sup>*School of Physical Sciences, University of Chinese Academy of Sciences, Beijing 100049, P.R. China*

<sup>4</sup>*Institute of Theoretical Physics, Chinese Academy of Sciences, Beijing 100190, P. R. China*

<sup>5</sup>*International Centre for Theoretical Physics Asia-Pacific, Beijing/Hangzhou, China*

We investigate constraints on neutrino non-standard interactions (NSIs) in the effective field theory framework, using data from the first measurement of solar  $^8\text{B}$  neutrinos via coherent elastic neutrino-nucleus scattering ( $\text{CE}\nu\text{NS}$ ) in the PandaX-4T experiment and the COHERENT experiment. In the PandaX-4T experiment, due to relatively large statistical uncertainties and measured  $\text{CE}\nu\text{NS}$  counts that significantly differ from the Standard Model predictions, its sensitivities to the neutrino NSIs are currently limited, compared to the COHERENT experiment. However, the PandaX-4T experiment is uniquely sensitive to the neutrino NSIs for the  $\tau$  flavor due to oscillation feature of the solar  $^8\text{B}$  neutrinos. We also assess how the experimental central value, exposure, and systematic uncertainties will affect the constraints on neutrino NSIs from various  $\text{CE}\nu\text{NS}$  measurements in the future.

## I. INTRODUCTION

In the Standard Model (SM), neutrinos interact with ordinary matter through the exchange of  $W$  and  $Z$  bosons. Neutrino non-standard interactions (NSIs) in the charged and neutral currents beyond the SM (BSM) were initially formulated by Lee-Yang [1] and Wolfenstein [2], respectively. While the detection of neutrinos in neutrino oscillation experiments only involves charged-current interactions, the coherent elastic neutrino-nucleus scattering ( $\text{CE}\nu\text{NS}$ ) [3] serves as a unique probe of the neutral-current neutrino NSIs, potentially arising from new mediators, such as  $Z'$  boson [4].

Despite the coherent enhancement of the  $\text{CE}\nu\text{NS}$  cross section, this process is difficult to detect due to small deposited energy. It was first observed in the COHERENT experiment using the CsI[Na] scintillation detector [5] and later argon [6] and germanium [7] detectors with neutrinos produced from the spallation neutron source (SNS). These results as well as the follow-up detection with a larger exposure of CsI[Na] [8] and other experimental efforts [9–18] have motivated diverse phenomenological studies [19–42], see also Refs. [43–45] for earlier studies and Ref. [46] for a recent review.

On the other hand, with the tremendous progress in the sensitivity of dark matter (DM) direct detection, it is anticipated that the DM experiments can detect neutrinos from astrophysical sources. These neutrinos exhibit nuclear recoil signatures resembling those of DM, which pose as irreducible backgrounds in DM direct detection and are often referred to as the “neutrino frog” [47–49].

This is not unexpected since the idea of detecting DM that scatters off nuclei [50] was inspired by the proposal to detect MeV-range neutrinos via  $\text{CE}\nu\text{NS}$  [51].

Recently, the solar  $^8\text{B}$  neutrino was measured through  $\text{CE}\nu\text{NS}$  in the PandaX-4T [52] and XENONnT [53] experiments with corresponding statistical significance of  $2.64\sigma$  and  $2.73\sigma$ , which signify the first step into the neutrino frog experimentally. Assuming the SM cross section of  $\text{CE}\nu\text{NS}$ , the signals are interpreted as the measurements of solar  $^8\text{B}$  neutrino flux of  $(8.4 \pm 3.1) \times 10^6 \text{ cm}^{-2} \text{ s}^{-1}$  and  $(4.7_{-2.3}^{+3.6}) \times 10^6 \text{ cm}^{-2} \text{ s}^{-1}$ , respectively, both of which are consistent with the standard solar model predictions [54–56] and the results from dedicated solar neutrino experiments [57–60].

In the SM, empirical nuclear form factors [61, 62] that parameterize the nuclear response are usually adopted to calculate the cross section of  $\text{CE}\nu\text{NS}$ . However, an improved treatment is necessary if neutrino NSIs are present, which is feasible in the effective field theory (EFT) approach [29, 35, 36]<sup>1</sup>, analogous to the situation of DM-nucleus scattering [63–71].

An end-to-end EFT framework [29] was developed and utilized to describe the  $\text{CE}\nu\text{NS}$  process from the new physics scale to the nuclear scale, which takes advantages of the heavy baryon chiral perturbation theory (HBChPT) [72] and multipole expansions for nuclear responses [73]<sup>2</sup>. Compared to the nuclear form factor approach, the EFTs enable controlled uncertainties in systematic power countings, which allows for potential

<sup>1</sup> For vector and axial-vector NSIs, one can also refine the  $\text{CE}\nu\text{NS}$  cross section by modifying the weak charge [4, 46].

<sup>2</sup> Indeed, the multipole analysis was applied to neutrino-nucleus scattering processes in the SM weak charged currents slightly before the proposal of  $\text{CE}\nu\text{NS}$  [74]. The effect of SM weak neutral currents in neutrino scattering off nuclei was later investigated in Ref. [75].

\* ligang65@mail.sysu.edu.cn

† songchuanqiang21@mails.ucas.ac.cn

‡ tangfenjie22@mails.ucas.ac.cn

§ jhyu@itp.ac.cn

theoretical improvements in nuclear shell-model calculations [35] and beyond [76].

In this work, we will investigate the sensitivities to neutrino NSIs in the EFT framework, including matching between several EFTs. We consider relevant dimension-6 operators in the low-energy effective field (LEFT) and QCD chiral Lagrangian with external sources and heavy baryon expansion, and finally match to nuclear response function to obtain the most stringent constraints from the measurement conducted with the CsI[Na] detector in the COHERENT experiment [8] and the first result of new physics using the measurement of solar  $^8\text{B}$  neutrinos by PandaX-4T [52].

The remainder of the paper is organized as follows. In Sec. II, we discuss the neutrino NSIs from quark level to the nucleon level using the LEFT and HBChPT. In Sec. III, we derive the CE $\nu$ NS cross section using the multipole expansions for nuclear responses. In Sec. IV, we evaluate the event rates of the CE $\nu$ NS signals in the COHERENT and PandaX-4T experiments (considering the matter effects in the neutrino propagation by using package PEANUTS), and obtain the constraints on the Wilson coefficients for specific neutrino flavors, which are interpreted as lower bounds on the NSI energy scale using the  $\chi^2$  analysis. Two-dimensional constraint on the NSI parameters is also obtained for the comparison of these two CE $\nu$ NS experiments. We have an assessment of the sensitivities of future measurements of solar  $^8\text{B}$  neutrinos via CE $\nu$ NS in DM detectors. We conclude in Sec. V. In the appendix, we provide details of the detector resolution and efficiency in COHERENT CsI measurement.

## II. NEUTRINO NON-STANDARD INTERACTIONS

The neutral-current (NC) neutrino-quark interactions can be parameterized as [2, 4, 38, 77, 78]

$$\mathcal{L}_{\text{NC}} \supset -2\sqrt{2}G_F \left[ \epsilon_{\alpha\beta}^{qL} (\bar{\nu}_\alpha \gamma^\mu P_L \nu_\beta) (\bar{q} \gamma_\mu P_L q) + \epsilon_{\alpha\beta}^{qR} (\bar{\nu}_\alpha \gamma^\mu P_L \nu_\beta) (\bar{q} \gamma_\mu P_R q) \right], \quad (1)$$

where  $P_{L/R} = (1 \mp \gamma_5)/2$ ,  $\alpha, \beta$  denote the flavors of neutrinos, and  $q = u, d$ ,  $G_F$  is the Fermi constant.

In the LEFT, the relevant effective Lagrangian is

$$\mathcal{L}_{\text{LEFT}} \supset \hat{\mathcal{C}}_{1,q}^{(6)} \mathcal{O}_{1,q}^{(6)} + \hat{\mathcal{C}}_{2,q}^{(6)} \mathcal{O}_{2,q}^{(6)}, \quad (2)$$

where the dimension-6 operators are defined as [29, 79]

$$\begin{aligned} \mathcal{O}_{1,q}^{(6)} &= (\bar{\nu}_\alpha \gamma_\mu P_L \nu_\beta) (\bar{q} \gamma^\mu q), \\ \mathcal{O}_{2,q}^{(6)} &= (\bar{\nu}_\alpha \gamma_\mu P_L \nu_\beta) (\bar{q} \gamma^\mu \gamma_5 q). \end{aligned} \quad (3)$$

The correspondence between the coefficients  $\epsilon_{\alpha\beta}^{qL(R)}$  and the Wilson coefficients  $\hat{\mathcal{C}}_{1,q}^{(6)}$  and  $\hat{\mathcal{C}}_{2,q}^{(6)}$  is

$$\epsilon_{\alpha\beta}^{qL/R} = -\frac{1}{2\sqrt{2}G_F} \left( \hat{\mathcal{C}}_{1,q}^{(6)} \mp \hat{\mathcal{C}}_{2,q}^{(6)} \right). \quad (4)$$

The SM contributions to the Wilson coefficients after integrating out the  $Z$  boson are [29, 46]

$$\hat{\mathcal{C}}_{1,u(d)}^{(6)} \Big|_{\text{SM}} = \mp \frac{G_F}{\sqrt{2}} \left( 1 - \frac{8(4)}{3} \sin^2 \theta_W \right) \delta_{\alpha\beta}, \quad (5)$$

$$\hat{\mathcal{C}}_{2,u(d)}^{(6)} \Big|_{\text{SM}} = \pm \frac{G_F}{\sqrt{2}} \delta_{\alpha\beta}. \quad (6)$$

where  $\theta_W$  is the weak mixing angle with  $\sin^2 \theta_W = 0.2312$  [80]. We consider contributions from neutrino NSIs, so that

$$\hat{\mathcal{C}}_i^{(6)} = \hat{\mathcal{C}}_i^{(6)} \Big|_{\text{SM}} + \hat{\mathcal{C}}_i^{(6)} \Big|_{\text{NSI}}. \quad (7)$$

The dimensionful Wilson coefficient can also be expressed as

$$\hat{\mathcal{C}}_i^{(6)} \Big|_{\text{NSI}} = \frac{1}{\Lambda_{\text{NSI}}^2} \mathcal{C}_i^{(6)} \Big|_{\text{NSI}}, \quad (8)$$

where  $\mathcal{C}_i^{(6)} \Big|_{\text{NSI}}$  is dimensionless, and the energy scale  $\Lambda_{\text{NSI}}$  is determined by the mass of mediator that is responsible for the neutrino NSIs<sup>3</sup>.

To obtain the neutrino-nucleus cross section of CE $\nu$ NS, we need to consider the matching in two steps [29, 35]: (1) from the quark level to the nucleon level; (2) from the nucleon level to the nucleus level. In the first step, the nucleons in the target are considered non-relativistic due to the small momentum exchange  $q$  compared to the nucleon mass. The interaction Lagrangian for the neutrinos and non-relativistic nucleons is

$$\mathcal{L}_{\text{NR}} = c_{i,N}^{(d)} \mathcal{O}_{i,N}^{(d)}, \quad (9)$$

where  $N = p, n$ , and  $d$  denotes the number of derivatives in the operator.

By using the HBChPT, the following neutrino-nucleon operators at leading order are obtained:

$$\mathcal{O}_{1,N}^{(0)} = (\bar{\nu}_\beta \gamma_\mu P_L \nu_\alpha) (v^\mu \bar{N}_v N_v), \quad (10)$$

$$\mathcal{O}_{2,N}^{(0)} = (\bar{\nu}_\beta \gamma_\mu P_L \nu_\alpha) (\bar{N}_v S^\mu N_v). \quad (11)$$

where  $N_v$  denotes the large component of the nucleon field, and  $v^\mu$  is the nucleon velocity, the spin operator  $S^\mu = \gamma_5 \gamma_\perp^\mu / 2$  with  $\gamma_\perp^\mu \equiv \gamma^\mu - v^\mu \not{v}$ . In the lab frame,  $v^\mu = (1, \vec{0})$ , and  $S^\mu = (0, \vec{\sigma}/2)$  with  $\vec{\sigma}$  being the Pauli matrices. Denoting  $p_1$  and  $p_2$  ( $k_1$  and  $k_2$ ) as the momenta of income and outcome neutrinos (nucleons), respectively, we can define the momentum transfer as  $q = p_1 - p_2$ .

From the quark-level interactions to the nucleon-level interactions, the matching conditions are expressed as<sup>4</sup>

$$c_{1,N}^{(0)} = \sum_{q=u,d} F_1^{q/N} \hat{\mathcal{C}}_{1,q}^{(6)}, \quad c_{2,N}^{(0)} = 2 \sum_{q=u,d} F_A^{q/N} \hat{\mathcal{C}}_{2,q}^{(6)}, \quad (12)$$

<sup>3</sup> For light mediator, there is additional momentum dependence from its propagator.

<sup>4</sup> Note that we use the symbol  $q$  to represent both the momentum transfer and the quark in the conventional manner.

where  $F_i$  denote the momentum-dependent nucleon form factors describing the hadronization of quark currents. We use the values of  $F_i$  evaluated at  $q^2 \rightarrow 0$  [71], which are accurate enough for our purpose,

$$\begin{aligned} F_1^{u/p} &= 2, & F_1^{d/p} &= 1, \\ F_A^{u/p} &= 0.897, & F_A^{d/p} &= -0.376. \end{aligned} \quad (13)$$

### III. CROSS SECTION OF CE $\nu$ NS

In the second step, the nuclear response to neutrino scattering needs to be considered at the nuclear level, which is described similarly to DM detection [68, 69]. In this framework, the many-body nuclear matrix elements are expanded using the multipole expansions [73] in the harmonic oscillator basis, and can be calculated in the nuclear shell model [35, 81].

To this end, we classify the Lagrangian terms according to charge operator ( $1_N$ ) and nuclear spin operator ( $\vec{S}$ ) [29]:

$$\mathcal{L}_{\text{NR}} = (\bar{\nu}_\alpha l_{0,N} P_L \nu_\beta) 1_N + (\bar{\nu}_\alpha \vec{l}_{5,N} P_L \nu_\beta) \cdot (2\vec{S}), \quad (14)$$

where the Dirac structures are given by

$$l_{0,N} = c_{1,N}^{(0)} \not{1}, \quad l_{5,N}^\mu = \frac{1}{2} c_{2,N}^{(0)} \gamma^\mu, \quad (15)$$

and  $\vec{l}_5$  in Eq. (14) is the spatial three-vector components of  $l_5^\mu$ .

The differential cross section in the rest frame of the target nucleus is [29]<sup>5</sup>

$$\frac{d\sigma}{dT_{\text{nr}}} = \frac{M}{8\pi E_\nu^2} |\overline{\mathcal{M}}|_{RW}^2, \quad (16)$$

where  $M$  is the target nucleus mass,  $E_\nu$  is the initial neutrino energy,  $T_{\text{nr}}$  is the nuclear recoil energy, and the spin-averaged amplitude square is expressed as

$$\begin{aligned} |\overline{\mathcal{M}}|_{RW}^2 &= \frac{4\pi}{2J_A + 1} \sum_{\tau, \tau'=0,1} \left( R_M^{\tau\tau'} W_M^{\tau\tau'} \right. \\ &\quad \left. + R_{\Sigma'}^{\tau\tau'} W_{\Sigma'}^{\tau\tau'} + R_{\Sigma''}^{\tau\tau'} W_{\Sigma''}^{\tau\tau'} \right). \end{aligned} \quad (17)$$

Here,  $J_A$  is the spin of the target nucleus,  $W_i$  denotes the nucleus response functions [68, 69], and the kinematic factors  $R_i$  are given by [29]

$$R_M^{\tau\tau'} = \text{Tr}(P_L \not{p}_1 \gamma_0 l_{0,\tau'}^\dagger \gamma_0 \not{p}_2 l_{0,\tau}), \quad (18)$$

$$R_{\Sigma'}^{\tau\tau'} = \text{Tr}(P_L \not{p}_1 \gamma_0 l_{5,\tau'}^{j\dagger} \gamma_0 \not{p}_2 l_{5,\tau}^i) \hat{q}^i \hat{q}^j, \quad (19)$$

$$R_{\Sigma''}^{\tau\tau'} = \text{Tr}(P_L \not{p}_1 \gamma_0 l_{5,\tau'}^{j\dagger} \gamma_0 \not{p}_2 l_{5,\tau}^i) (\delta^{ij} - \hat{q}^i \hat{q}^j), \quad (20)$$

where  $\tau, \tau'$  are the isospin indices,  $\hat{q} \equiv \vec{q}/|\vec{q}|$ , and  $i, j = 1, 2, 3$ . In the isospin basis,  $l_{0,\tau} = [l_{0,p} + (-1)^\tau l_{0,n}]/2$  and  $l_{5,\tau}^\mu = [l_{5,p}^\mu + (-1)^\tau l_{5,n}^\mu]/2$ .

<sup>5</sup> We have corrected a missing factor of 1/8 in Eq.(3.23) of Ref. [29], and have verified it by comparing the SM result with the calculation using the nuclear form factor [43, 46].

## IV. EVENT RATES AND CONSTRAINTS

In the CE $\nu$ NS experiments, neutrinos from the source will interact with detector target nuclei, causing nucleus recoils. The resulting signal can be translated into the event rate. In the following, we will investigate constraints on neutrino NSIs from the measurements by the COHERENT and PandaX-4T experiments.

### A. Constraints from COHERENT

We first consider the measurements of the CE $\nu$ NS process in the COHERENT experiment using CsI[Na] [8]<sup>6</sup>. The differential event rate per target for neutrino flavor  $\nu_\alpha = \nu_e, \nu_\mu, \bar{\nu}_\mu$  is expressed as [29, 76]:

$$\frac{dR_{\nu_\alpha}}{dT_{\text{nr}}} = \int_{E_{\nu,\text{min}}}^{E_{\nu,\text{max}}} dE_\nu \Phi_{\nu_\alpha}(E_\nu) \frac{d\sigma}{dT_{\text{nr}}}, \quad (21)$$

where  $d\sigma/dT_{\text{nr}}$  is the differential cross section given in Eq. (16). The minimum initial neutrino energy is  $E_{\nu,\text{min}} \simeq \sqrt{MT_{\text{nr}}/2}$ , where  $M$  is the nucleus mass. The upper integration limit is given by the maximal energy of initial neutrinos produced in  $\pi^+ \rightarrow \nu_\mu (\mu^+ \rightarrow e^+ \nu_e \bar{\nu}_\mu)$ . For  $\nu_e$  and  $\bar{\nu}_\mu$ ,  $E_{\nu,\text{max}} = m_\mu/2 \simeq 52.8$  MeV, while for  $\nu_\mu$ ,  $E_{\nu,\text{max}} = (m_\pi^2 - m_\mu^2)/(2m_\pi) \simeq 30$  MeV [27, 40], where  $m_\mu$  and  $m_\pi$  are the mass of the muon and pion, respectively.

The total neutrino fluxes are described by the Michel spectrum [20, 45]

$$\Phi_{\nu_e}(E_\nu) = \mathcal{N} \frac{192E_\nu^2}{m_\mu^3} \left( \frac{1}{2} - \frac{E_\nu}{m_\mu} \right), \quad (22)$$

$$\Phi_{\bar{\nu}_\mu}(E_\nu) = \mathcal{N} \frac{64E_\nu^2}{m_\mu^3} \left( \frac{3}{4} - \frac{E_\nu}{m_\mu} \right), \quad (23)$$

$$\Phi_{\nu_\mu}(E_\nu) = \mathcal{N} \delta \left( E_\nu - \frac{m_\pi^2 - m_\mu^2}{2m_\pi} \right), \quad (24)$$

where  $\delta$  is the Dirac  $\delta$ -function, and the overall factor  $\mathcal{N} \equiv rN_{\text{POT}}/(4\pi L^2)$  depends on the number of neutrinos ( $r$ ) that are produced for each proton on target (POT), the number of protons on target ( $N_{\text{POT}}$ ) and the distance between the source and the detector ( $L$ ). For the CsI[Na] detector in COHERENT experiment,  $r = 0.0848$ ,  $N_{\text{POT}} = 3.198 \times 10^{23}$  and  $L = 19.3$  m [8].

The time-integrated expected number of CE $\nu$ NS events in the  $i$ th bin of the number of photoelectrons

<sup>6</sup> We do not consider the COHERENT measurement using Ar detector [6] since its sensitivity cannot compete with that CsI detector, even though the combination of these measurements can break degeneracy between different NSI parameter combinations [41].

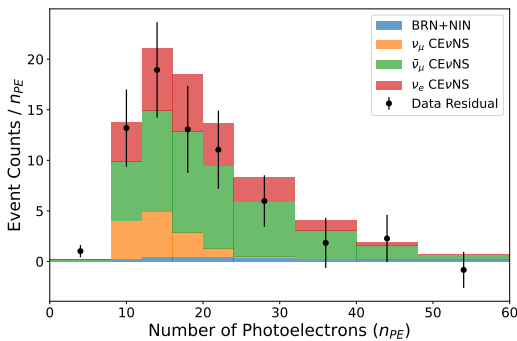


Figure 1: The comparison of the total expected event counts for CE $\nu$ NS events in the SM calculated using the nuclear response functions, with the experimental data (black points with error bars) collected with CsI[Na] detector by the COHERENT Collaboration [82]. The numbers of events from different flavors are shown.

(PEs) for the flavor  $\nu_\alpha$  is given by [27, 32, 40, 41]

$$N_{\nu_\alpha}^i = n_N \sum_{x=\text{Cs,I}} \eta_x \langle \varepsilon_T \rangle_{\nu_\alpha} \int_{n_{\text{PE}}^i}^{n_{\text{PE}}^{i+1}} dn_{\text{PE}} \varepsilon(n_{\text{PE}}) \times \int_{T_{\text{nr,min}}}^{T_{\text{nr,max}}} dT_{\text{nr}} P(n_{\text{PE}}) \left. \frac{dR_{\nu_\alpha}}{dT_{\text{nr}}} \right|_x, \quad (25)$$

where we have taken into account the recoils of Cs and I with the fractions  $\eta_{\text{Cs}} = 51\%$  and  $\eta_{\text{I}} = 49\%$ , respectively. The number of target nuclei in the detector is  $n_N \equiv N_A M_{\text{det}} / M_T$ , where  $M_{\text{det}} = 14.6$  kg is the detector active mass,  $M_T = 259.8$  g/mol is the molar mass of CsI, and  $N_A$  denotes the Avogadro number. The detector energy resolution  $P(n_{\text{PE}})$  and efficiency  $\varepsilon(n_{\text{PE}})$  as well as the average time efficiency  $\langle \varepsilon_T \rangle_{\nu_\alpha}$  are described in Appendix A.

In Fig. 1, we compare the expected number of CE $\nu$ NS events in the SM as a function of  $n_{\text{PE}}$ , which is calculated using the nuclear response functions described in Sec. III, with the experimental data from COHERENT. The contributions from different neutrino fluxes are included.

To constrain the neutrino NSIs, we perform the binned  $\chi^2$  analysis using the following least-squares function [27, 83],

$$\chi^2 = \sum_{i=1}^9 \frac{[N_{\text{meas}}^i - N_{\text{CE}\nu\text{NS}}^i(1 + \alpha) - N_{\text{BRN+NIN}}^i(1 + \beta)]^2}{(\sigma_{\text{stat}}^i)^2} + \left( \frac{\alpha}{\sigma_\alpha} \right)^2 + \left( \frac{\beta}{\sigma_\beta} \right)^2, \quad (26)$$

where  $N_{\text{meas}}^i$  and  $N_{\text{BRN+NIN}}^i$  represent the measured number of CE $\nu$ NS events, and the expected number of beam-related neutron (BRN) and neutrino-induced neutron (NIN) background events in the  $i$ th bin of  $n_{\text{PE}}$ , respectively. The associated statistical uncertainty is  $\sigma_{\text{stat}}^i = \sqrt{N_{\text{meas}}^i + N_{\text{BRN+NIN}}^i}$ . The expected number of

CE $\nu$ NS events is given by

$$N_{\text{CE}\nu\text{NS}}^i = N_{\nu_e}^i + N_{\nu_\mu}^i + N_{\bar{\nu}_\mu}^i, \quad (27)$$

which depends on the neutrino NSIs.

The relative systematic uncertainties from the quenching factor (3.8%), neutrino flux (10%) and signal acceptance (4.1%) [8, 41], and the response functions (5%) are considered<sup>7</sup>, which lead to the total uncertainty  $\sigma_\alpha = 0.125$ . Besides,  $\sigma_\beta = \sqrt{\sigma_{\text{BRN}}^2 + \sigma_{\text{NIN}}^2}$  with the uncertainties of BRN and NIN backgrounds are  $\sigma_{\text{BRN}} = 0.25$  and  $\sigma_{\text{NIN}} = 0.35$ , respectively.

The quantity  $\chi^2$  is minimized over the systematic nuisance parameters  $\alpha$  and  $\beta$ , so that we can derive the 90% confidence level (C.L.) bounds on the Wilson coefficients of neutrino NSIs by requiring  $\Delta\chi^2 \equiv \chi^2 - \chi_{\text{min}}^2 \leq 2.71$ . In Eq. (8), assuming  $C_i^{(6)} \Big|_{\text{NSI}} = 1$  and summing over the fluxes of  $\nu_\mu$  and  $\bar{\nu}_\mu$ , we obtain the one-parameter-a-time lower bounds on  $\Lambda_{\text{NSI}}$  for specific flavors, which are presented in Table I.

$\Lambda_{\text{NSI}}/\text{GeV}$	$\nu_e$	$\nu_\mu$
$\hat{C}_{1,u}^{(6)}$	390	395
$\hat{C}_{1,d}^{(6)}$	407	414
$\hat{C}_{2,u}^{(6)}$	44.7	68.4
$\hat{C}_{2,d}^{(6)}$	26.4	40.9

Table I: Lower bounds on  $\Lambda_{\text{NSI}}$  in units of GeV for the Wilson coefficients  $\hat{C}_i^{(6)} \Big|_{\text{NSI}} = \hat{C}_i^{(6)} - \hat{C}_i^{(6)} \Big|_{\text{SM}}$  from COHERENT [8].

## B. Constraints from PandaX-4T

The recent measurements of solar  $^8\text{B}$  neutrinos in the CE $\nu$ NS process [52, 53, 84] can also impose constraints on the neutrino NSIs. In this work, we consider the results of the PandaX-4T experiment using the liquid xenon [52].

The differential event rate per target for neutrino flavor  $\nu_\alpha = \nu_e, \nu_\mu, \nu_\tau$  is expressed as

$$\frac{dR_{\nu_\alpha}}{dT_{\text{nr}}} = \int_{E_{\nu,\text{min}}}^{E_{\nu,\text{max}}} dE_\nu \Phi_{\nu_\alpha}(E_\nu) \frac{d\sigma}{dT_{\text{nr}}}, \quad (28)$$

where the minimum neutrino energy  $E_{\nu,\text{min}} \simeq \sqrt{MT_{\text{nr}}/2}$  with  $M$  the mass of  $^{131}\text{Xe}$ , and the maximum energy  $E_{\nu,\text{max}}$  is about 16 MeV [55].

The solar  $^8\text{B}$  neutrino  $\nu_e$  is produced in the Sun, and then propagates to the Earth. The total flux of neutrino

<sup>7</sup> It is noted that in the approach of nuclear form factor, the relative systematic uncertainty is about 5% [32]. Here, we assume that the uncertainties associated with the response functions are comparable.

$\nu_\alpha$  detected at the Earth is defined as

$$\Phi_{\nu_\alpha}(E_\nu) = \frac{\mathcal{E}}{M_{\text{det}}} \langle P_{\nu_\alpha} \rangle \phi(^8\text{B}), \quad (29)$$

where  $\mathcal{E}$  and  $M_{\text{det}}$  denote the exposure and detector active mass, respectively, and  $\phi(^8\text{B}) = 5.46(1 \pm 0.12) \times 10^6 \text{ cm}^{-2}\text{s}^{-1}$  is the predicted solar  $^8\text{B}$  neutrino flux [54]<sup>8</sup>.  $\langle P_{\nu_\alpha} \rangle$  is the probability of solar neutrino  $\nu_e$  to manifest as  $\nu_\alpha$  at the Earth averaged over the exposure.

Due to the neutrino oscillation, the flavor composition of solar neutrinos detected at the Earth differs from that produced in the Sun. In the analysis, we use the package PEANUTS [85] to compute  $\langle P_{\nu_\alpha} \rangle$  with matter effects in the neutrino propagation being included, which are shown in Fig. 2 for different flavors of neutrinos.

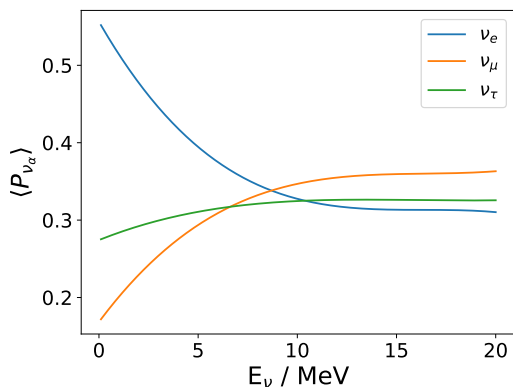


Figure 2: The probabilities of various neutrino fluxes at the Earth, averaged over the exposure period, are detailed.

The expected number of  $\text{CE}\nu\text{NS}$  events for the flavor  $\nu_\alpha$  is given by [42],

$$N_{\nu_\alpha} = n_N \int_{T_{\text{nr},\text{min}}}^{T_{\text{nr},\text{max}}} dT_{\text{nr}} \varepsilon(T_{\text{nr}}) \frac{dR_\alpha}{dT_{\text{nr}}}, \quad (30)$$

where  $\varepsilon(T_{\text{nr}})$  is the detection efficiency, which depends on the nuclear recoil function. The number of target nuclei ( $^{131}\text{Xe}$ ) in the detector of the PandaX-4T experiment is  $n_N \equiv N_A M_{\text{det}}/M_T$  with the molar mass  $M_T = 131.29 \text{ g/mol}$ .

Two datasets are collected by PandaX-4T, which differ in the energy threshold, as displayed in Table II. Note that the numbers of signal events for the pair data (3.5) and US2 data (75) are obtained from the combined likelihood fit [52]. Given the smaller number of signal events in paired data, we only consider the US2 data. The exposure in Eq. (29) is thus given by  $\mathcal{E} = 1.04 \text{ tonne} \cdot \text{year}$ .

PandaX-4T data	paired	US2
energy threshold	1.1 keV	0.33 keV
total exposure	1.25 tonne-year	1.04 tonne-year
event number	3.5	75

Table II: The experimental data of detecting solar  $^8\text{B}$  neutrinos in the  $\text{CE}\nu\text{NS}$  process by PandaX-4T [52]. The energy thresholds, total exposures, and numbers of signal events for the paired and US2 data are given.

In the analysis by the PandaX-4T Collaboration [52], the signals are interpreted in terms of the measured solar  $^8\text{B}$  neutrino flux assuming the SM cross section of  $\text{CE}\nu\text{NS}$ , which is  $(8.4 \pm 3.1) \times 10^6 \text{ cm}^{-2}$  with the relative statistical uncertainty being 37%. Therefore, for our purpose, instead of taking the number of signal events post the combined likelihood fit, we calculate the number of signal events for the US2 data using the signal efficiency from Figure 1 of Ref. [52]. We obtain the measured number of  $\text{CE}\nu\text{NS}$  events  $N_{\text{meas}} = 69.1$  with the statistic uncertainty  $\sigma_{\text{stat}} = 0.37 \times N_{\text{meas}}$ .

To constrain the neutrino NSIs, we perform the single-bin  $\chi^2$  analysis [83],

$$\chi^2 = \frac{[N_{\text{meas}} - N_{\text{CE}\nu\text{NS}}(1 + \alpha)]^2}{\sigma_{\text{stat}}^2} + \left(\frac{\alpha}{\sigma_\alpha}\right)^2. \quad (31)$$

Here, the expected number of  $\text{CE}\nu\text{NS}$  events is given by

$$N_{\text{CE}\nu\text{NS}} = N_{\nu_e} + N_{\nu_\mu} + N_{\nu_\tau}, \quad (32)$$

which depends on the neutrino NSIs, and the SM prediction  $N_{\text{CE}\nu\text{NS}}|_{\text{SM}} = 44.9$  calculated using the solar  $^8\text{B}$  neutrino flux  $\phi(^8\text{B}) = 5.46(1 \pm 0.12) \times 10^6 \text{ cm}^{-2}\text{s}^{-1}$  [54]. The relative systematic uncertainties from the selection efficiency (12%), signal modeling (17%) and solar  $^8\text{B}$  neutrino flux (12%) [52, 54], and the response functions (5%) are considered, which lead to the total uncertainty  $\sigma_\alpha = 0.245$ .

Again,  $\chi^2$  is minimized over the nuisance parameter  $\alpha$  to derive the 90% C.L. limits on the Wilson coefficients by requiring  $\Delta\chi^2 \equiv \chi^2 - \chi_{\text{min}}^2 \leq 2.71$ . In Eq. (8), assuming  $\mathcal{C}_i^{(6)}|_{\text{NSI}} = 1$ , we obtain the one-parameter-a-time lower bounds on  $\Lambda_{\text{NSI}}$  for specific flavors, which are presented in Table III.

$\Lambda_{\text{NSI}}/\text{GeV}$	$\nu_e$	$\nu_\mu$	$\nu_\tau$
$\hat{\mathcal{C}}_{1,u}^{(6)}$	287.46	289.61	286.70
$\hat{\mathcal{C}}_{1,d}^{(6)}$	304.61	306.88	303.80
$\hat{\mathcal{C}}_{2,u}^{(6)}$	14.70	14.81	14.60
$\hat{\mathcal{C}}_{2,d}^{(6)}$	23.32	23.48	23.15

Table III: Lower bounds on  $\Lambda_{\text{NSI}}$  in units of GeV for the Wilson coefficients  $\hat{\mathcal{C}}_i^{(6)}|_{\text{NSI}} = \hat{\mathcal{C}}_i^{(6)} - \hat{\mathcal{C}}_i^{(6)}|_{\text{SM}}$  from PandaX-4T [52].

<sup>8</sup> The predictions by the other groups based on the standard solar model can be found in Refs. [55, 56].

Owing to the neutrino oscillation, a significant portion of the solar neutrino fluxes reaching the Earth are com-

posed of  $\nu_\tau$  as depicted in Fig. 2. Therefore, the  $\text{CE}\nu\text{NS}$  measurement of PandaX-4T can give unique constraints on the neutrino NSIs for the  $\tau$  flavor as shown in the last column of Table III. For the  $e$  and  $\mu$  flavors, the measurement of COHERENT CsI provides more stringent constraints on the Wilson coefficients of NSIs than the constraints provided by PandaX-4T.

For comparison, we also obtain the two-dimensional constraint on the neutrino NSI parameters  $\epsilon_{ee}^{uV}$  and  $\epsilon_{ee}^{dV}$ , which are defined as [46]

$$\epsilon_{ee}^{qV} = \frac{-1}{\sqrt{2}G_F} \mathcal{C}_{1,q}^{(6)} \Big|_{\text{NSI}}. \quad (33)$$

By requiring  $\Delta\chi^2 \leq 4.61$ , we obtain the 90% C.L. allowed regions in Fig. 3. Note that our fitted result using the COHERENT CsI measurement agrees with Ref. [41]. It is shown that the constraints on  $\epsilon_{ee}^{uV}$  and  $\epsilon_{ee}^{dV}$  from the  $\text{CE}\nu\text{NS}$  measurement by PandaX-4T are weaker than those from COHERENT.

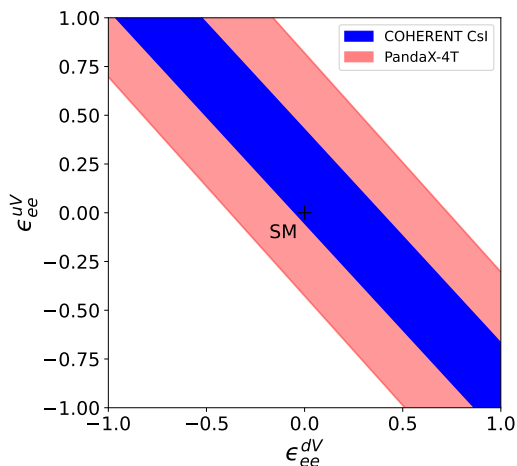


Figure 3: The 90% C.L. allowed regions of  $\epsilon_{ee}^{uV}$  and  $\epsilon_{ee}^{dV}$  by the measurements in the COHERENT CsI [8] and PandaX-4T [52] experiments, as depicted in blue and red colors, respectively.

We find that the central value of experimentally measured  $\text{CE}\nu\text{NS}$  counts has a significant impact on the constraints on the NSI parameters<sup>9</sup>. To understand it, we present the  $\Delta\chi^2$  distribution as a function of the  $\text{CE}\nu\text{NS}$  counts in Fig. 4, using the US2 data from PandaX-4T. The upper limit of the  $\text{CE}\nu\text{NS}$  counts with  $\Delta\chi^2 \leq 4.61$  determines the boundaries of the blue bands in Fig. 5. It is verified that with the central value unchanged, the sensitivity of PandaX-4T shows a mild improvement for  $\sim 5$  times larger exposure.

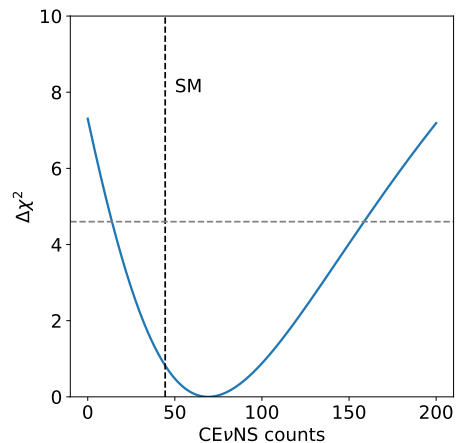


Figure 4: The distribution of  $\Delta\chi^2$  as a function of the  $\text{CE}\nu\text{NS}$  counts. The SM prediction of the  $\text{CE}\nu\text{NS}$  counts is 44.9, located at the endpoint of the black dotted line. The central value of measured  $\text{CE}\nu\text{NS}$  counts in the PandaX-4T experiment (US2 data) is 69.1, located at the minimum of  $\Delta\chi^2$  distribution. The gray line corresponds to  $\Delta\chi^2 = 4.61$ .

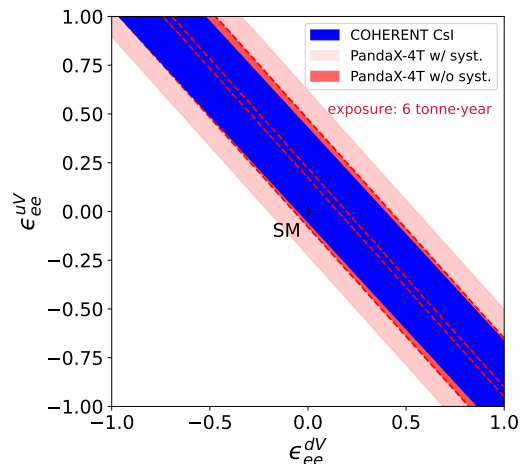


Figure 5: The 90% C.L. allowed regions of  $\epsilon_{ee}^{uV}$  and  $\epsilon_{ee}^{dV}$  by the COHERENT CsI measurement (blue) and anticipated measurements by PandaX-4T assuming the experimental central value  $N_{\text{meas}} = N_{\text{CE}\nu\text{NS}}|_{\text{SM}} = 44.9$  and exposure  $\mathcal{E} = 6 \text{ tonne} \cdot \text{year}$ . The lighter and darker red regions are obtained with the systematic uncertainty  $\sigma_\alpha = 0.245$  and 0, respectively.

We further assess the sensitivities of future solar  $^8\text{B}$  neutrino measurements via  $\text{CE}\nu\text{NS}$  in DM detectors, leveraging the current results from PandaX-4T as a reference. In Fig. 5, we show the projected constraints on the NSI parameters under the assumption of  $N_{\text{meas}} = N_{\text{CE}\nu\text{NS}}|_{\text{SM}} = 44.9$  and  $\mathcal{E} = 6 \text{ tonne} \cdot \text{year}$ . We consider two cases with the total systematic uncertainty  $\sigma_\alpha = 0.245$  being included or not. The resulting constraints are represented in lighter red and darker red

<sup>9</sup> It is noted that the central value measured by XENONnT is slightly smaller than the SM prediction, whereas the associated statistical uncertainty is larger compared to PandaX-4T [53].

bands with solid and dashed boundaries, respectively. One can observe that the anticipated constraint from PandaX-4T with the systematic uncertainties is weaker than that from COHERENT. If in the future the systematic uncertainties are well controlled, with the assumption that they are negligible, we could achieve a sensitivity comparable to that of the COHERENT CsI measurement.

## V. CONCLUSION

In this work, we have studied the constraints on the neutrino non-standard interactions (NSIs) using the latest  $\text{CE}\nu\text{NS}$  measurements in the COHERENT and PandaX-4T experiments. The cross section of  $\text{CE}\nu\text{NS}$  is calculated within an end-to-end effective field theory framework. In this approach, the dimension-6 operators in the low-energy EFT are matched to hadronic operators in the heavy baryon chiral perturbation theory, while the nuclear response of target nuclei is described using multipole expansions.

We have performed the  $\chi^2$  analyses of the  $\text{CE}\nu\text{NS}$  events observed in the CsI[Na] detector of COHERENT and PandaX-4T, and have derived the one-parameter-at-time lower bounds on the NSI scale for specific neutrino flavors. We have found that the constraints for the  $e$  and  $\mu$  flavors from COHERENT are more stringent than those from PandaX-4T, while the latter provides unique sensitivities to the neutrino NSIs for the  $\tau$  flavor due to the oscillation of solar  $^8\text{B}$  neutrinos propagating from the Sun to the Earth (considering the matter effects in the neutrino propagation by using package PEANUTS). Besides, we have compared the two-dimensional constraints on the NSI parameters for the  $e$  flavor from COHERENT and PandaX-4T, and have obtained that the sensitivity of PandaX-4T is limited by the central value of measured  $\text{CE}\nu\text{NS}$  counts.

Moreover, we have assessed the measurements of the solar  $^8\text{B}$  neutrinos via  $\text{CE}\nu\text{NS}$  in dark matter detectors, leveraging the current results from PandaX-4T as a reference. Assuming that the central value of measured  $\text{CE}\nu\text{NS}$  counts aligns with the SM prediction, the sensitivity is significantly improved for the exposure of 6 tonne · year, and is comparable to that imposed by the COHERENT CsI measurement if the systematic uncertainties are further disregarded.

**Note added:** After this paper was finished, another paper [86] appeared, which has some overlap of our work. However, we use an end-to-end EFT framework to investigate the neutrino NSIs sensitivities, and we emphasize that it is important to include systematic uncertainties in the analysis.

## ACKNOWLEDGMENTS

We would like to express our gratitude to Yu-Feng Li for the valuable help with the  $\chi^2$  fitting of the COHERENT data. GL also thanks Xun-Jie Xu for useful correspondence regarding Ref. [43]. FT thanks Ningqiang Song for the discussion on the solar neutrino and Bing-Long Zhang for the discussion on numerical calculations. This work is supported by the National Science Foundation of China under Grants No. 12347105, No. 12375099 and No. 12047503, and the National Key Research and Development Program of China Grant No. 2020YFC2201501, No. 2021YFA0718304. GL is also supported by the Guangdong Basic and Applied Basic Research Foundation (2024A1515012668), and SYSU startup funding.

### Appendix A: Detector resolution and efficiency in COHERENT CsI measurement

In Eq. (25), the number of PEs is [8, 32]

$$n_{\text{PE}} = 13.35 \frac{T_{ee}}{\text{keV}}, \quad (\text{A1})$$

where the true electron-equivalent recoil energy  $T_{ee}$  is related to the true nuclear recoil energy as

$$T_{ee} = f_Q(T_{\text{nr}})T_{\text{nr}}. \quad (\text{A2})$$

The quenching factor  $f_Q(T_{\text{nr}})$  can be parameterized as [87]

$$f_Q(T_{\text{nr}}) = k_0 + k_1 T_{\text{nr}} + k_2 T_{\text{nr}}^2 + k_3 T_{\text{nr}}^3, \quad (\text{A3})$$

where the parameters  $k_0 = 0.05546$ ,  $k_1 = 4.307$ ,  $k_2 = -111.7$  and  $k_3 = 840.4$ .

The detector energy resolution  $P(n_{\text{PE}})$  is modeled with the gamma function,

$$P(n_{\text{PE}}) = \frac{(a(1+b))^{1+b}}{\Gamma(1+b)} n_{\text{PE}}^b e^{-a(1+b)n_{\text{PE}}}, \quad (\text{A4})$$

where  $a = 0.0749 \text{ keV}/E_{ee}$  and  $b = 9.56E_{ee}/\text{keV}$ .

The reconstructed energy and time are uncorrelated, thus allowing us to deal with the energy and time efficiency independently [8],

$$\varepsilon_E(n_{\text{PE}}) = \frac{a_1}{1 + e^{-b_1(n_{\text{PE}} - c_1)}} + d_1, \quad (\text{A5})$$

$$\varepsilon_T(t_{\text{rec}}) = \begin{cases} 1, & t_{\text{rec}} < a_2, \\ e^{-b_2(t_{\text{rec}} - a_2)}, & t_{\text{rec}} \geq a_2, \end{cases} \quad (\text{A6})$$

where the parameters are  $a_1 = 1.32$ ,  $b_1 = 0.285$ ,  $c_1 = 10.9$ ,  $d_1 = -0.333$ , and  $a_2 = 0.52 \mu\text{s}$ ,  $b_2 = 0.0494/\mu\text{s}$  [8].

The efficiency  $\varepsilon(n_{\text{PE}})$  has been implemented in the integration over  $n_{\text{PE}}$  in Eq. (25). On the other hand, we

consider the average time efficiency

$$\langle \varepsilon_T \rangle_{\nu_\alpha} \equiv \frac{\sum_j \int_{t_{\text{rec}}^i}^{t_{\text{rec}}^{j+1}} dt_{\text{rec}} \varepsilon_T(t_{\text{rec}}) N_{\nu_\alpha}^j(t_{\text{rec}})}{\sum_j \int_{t_{\text{rec}}^i}^{t_{\text{rec}}^{j+1}} dt_{\text{rec}} N_{\nu_\alpha}^j(t_{\text{rec}})}, \quad (\text{A7})$$

where  $N_{\nu_\alpha}^j(t_{\text{rec}})$  represents the  $n_{\text{PE}}$ -integrated expected

number of the SM CE $\nu$ NS events in the reconstructed time  $t_{\text{rec}}$  for each flavor of neutrino flux depicted in the right panel of Figure 1 in Ref. [8]. Due to variations in neutrino arrival times, the time efficiencies for different flavors are distinct,  $\langle \varepsilon_T \rangle_{\nu_\mu} = 0.994$ ,  $\langle \varepsilon_T \rangle_{\bar{\nu}_\mu} = 0.918$  and  $\langle \varepsilon_T \rangle_{\nu_e} = 0.92$ .

- 
- [1] T. D. Lee and C.-N. Yang, *Phys. Rev.* **104**, 254 (1956).  
[2] L. Wolfenstein, *Phys. Rev. D* **17**, 2369 (1978).  
[3] D. Z. Freedman, *Phys. Rev. D* **9**, 1389 (1974).  
[4] J. Barranco, O. G. Miranda, and T. I. Rashba, *JHEP* **12**, 021 (2005), arXiv:hep-ph/0508299.  
[5] D. Akimov et al. (COHERENT), *Science* **357**, 1123 (2017), arXiv:1708.01294 [nucl-ex].  
[6] D. Akimov et al. (COHERENT), *Phys. Rev. Lett.* **126**, 012002 (2021), arXiv:2003.10630 [nucl-ex].  
[7] S. Adamski et al., (2024), arXiv:2406.13806 [hep-ex].  
[8] D. Akimov et al. (COHERENT), *Phys. Rev. Lett.* **129**, 081801 (2022), arXiv:2110.07730 [hep-ex].  
[9] A. Aguilar-Arevalo et al. (CONNIE), *Phys. Rev. D* **100**, 092005 (2019), arXiv:1906.02200 [physics.ins-det].  
[10] H. Bonet et al. (CONUS), *Phys. Rev. Lett.* **126**, 041804 (2021), arXiv:2011.00210 [hep-ex].  
[11] I. Alekseev et al. ( $\nu$ GeN), *Phys. Rev. D* **106**, L051101 (2022), arXiv:2205.04305 [nucl-ex].  
[12] J. Colaresi, J. I. Collar, T. W. Hossbach, C. M. Lewis, and K. M. Yocum, *Phys. Rev. Lett.* **129**, 211802 (2022), arXiv:2202.09672 [hep-ex].  
[13] C. Su, Q. Liu, and T. Liang (CLOVERS, CE $\nu$ NS@CSNS), *Phys. Sci. Forum* **8**, 19 (2023), arXiv:2303.13423 [physics.ins-det].  
[14] C. Augier et al. (Ricochet), *Nucl. Instrum. Meth. A* **1057**, 168765 (2023), arXiv:2304.14926 [physics.ins-det].  
[15] N. Ackermann et al., (2024), arXiv:2401.07684 [hep-ex].  
[16] L. T. Yang, Y. F. Liang, and Q. Yue, *PoS TAUP2023*, 296 (2024).  
[17] C. Cai et al., (2024), arXiv:2405.05554 [hep-ex].  
[18] X. Xiao, “Cicenns: a 300-kg csi(na) detector for coherent elastic neutrino-nucleus scattering,” (2024).  
[19] P. Coloma, M. C. Gonzalez-Garcia, M. Maltoni, and T. Schwetz, *Phys. Rev. D* **96**, 115007 (2017), arXiv:1708.02899 [hep-ph].  
[20] J. Liao and D. Marfatia, *Phys. Lett. B* **775**, 54 (2017), arXiv:1708.04255 [hep-ph].  
[21] M. Cadeddu, C. Giunti, Y. F. Li, and Y. Y. Zhang, *Phys. Rev. Lett.* **120**, 072501 (2018), arXiv:1710.02730 [hep-ph].  
[22] S.-F. Ge and I. M. Shoemaker, *JHEP* **11**, 066 (2018), arXiv:1710.10889 [hep-ph].  
[23] D. Aristizabal Sierra, N. Rojas, and M. H. G. Tytgat, *JHEP* **03**, 197 (2018), arXiv:1712.09667 [hep-ph].  
[24] E. Ciuffoli, J. Evslin, Q. Fu, and J. Tang, *Phys. Rev. D* **97**, 113003 (2018), arXiv:1801.02166 [physics.ins-det].  
[25] Y. Farzan, M. Lindner, W. Rodejohann, and X.-J. Xu, *JHEP* **05**, 066 (2018), arXiv:1802.05171 [hep-ph].  
[26] J. Billard, J. Johnston, and B. J. Kavanagh, *JCAP* **11**, 016 (2018), arXiv:1805.01798 [hep-ph].  
[27] D. Aristizabal Sierra, V. De Romeri, and N. Rojas, *Phys. Rev. D* **98**, 075018 (2018), arXiv:1806.07424 [hep-ph].  
[28] M. Cadeddu and F. Dordei, *Phys. Rev. D* **99**, 033010 (2019), arXiv:1808.10202 [hep-ph].  
[29] W. Altmannshofer, M. Tammaro, and J. Zupan, *JHEP* **09**, 083 (2019), [Erratum: *JHEP* **11**, 113 (2021)], arXiv:1812.02778 [hep-ph].  
[30] O. G. Miranda, G. Sanchez Garcia, and O. Sanders, *Adv. High Energy Phys.* **2019**, 3902819 (2019), [Erratum: *Adv.High Energy Phys.* **2022**, 9874517 (2022)], arXiv:1902.09036 [hep-ph].  
[31] D. Aristizabal Sierra, V. De Romeri, and N. Rojas, *JHEP* **09**, 069 (2019), arXiv:1906.01156 [hep-ph].  
[32] D. K. Papoulias, *Phys. Rev. D* **102**, 113004 (2020), arXiv:1907.11644 [hep-ph].  
[33] C. Giunti, *Phys. Rev. D* **101**, 035039 (2020), arXiv:1909.00466 [hep-ph].  
[34] B. C. Canas, E. A. Garces, O. G. Miranda, A. Parada, and G. Sanchez Garcia, *Phys. Rev. D* **101**, 035012 (2020), arXiv:1911.09831 [hep-ph].  
[35] M. Hoferichter, J. Menéndez, and A. Schwenk, *Phys. Rev. D* **102**, 074018 (2020), arXiv:2007.08529 [hep-ph].  
[36] W. Skiba and Q. Xia, *JHEP* **10**, 102 (2022), arXiv:2007.15688 [hep-ph].  
[37] M. Cadeddu, N. Cargioli, F. Dordei, C. Giunti, Y. F. Li, E. Picciau, and Y. Y. Zhang, *JHEP* **01**, 116 (2021), arXiv:2008.05022 [hep-ph].  
[38] Y. Du, H.-L. Li, J. Tang, S. Vihonen, and J.-H. Yu, *Phys. Rev. D* **105**, 075022 (2022), arXiv:2106.15800 [hep-ph].  
[39] A. Dasgupta, S. K. Kang, and J. E. Kim, *JHEP* **11**, 120 (2021), arXiv:2108.12998 [hep-ph].  
[40] M. Atzori Corona, M. Cadeddu, N. Cargioli, F. Dordei, C. Giunti, Y. F. Li, C. A. Ternes, and Y. Y. Zhang, *JHEP* **09**, 164 (2022), arXiv:2205.09484 [hep-ph].  
[41] V. De Romeri, O. G. Miranda, D. K. Papoulias, G. Sanchez Garcia, M. Tórtola, and J. W. F. Valle, *JHEP* **04**, 035 (2023), arXiv:2211.11905 [hep-ph].  
[42] Y.-Y. Li, Y.-F. Li, and S.-Y. Xia, (2024), arXiv:2406.07477 [hep-ph].  
[43] M. Lindner, W. Rodejohann, and X.-J. Xu, *JHEP* **03**, 097 (2017), arXiv:1612.04150 [hep-ph].  
[44] J. B. Dent, B. Dutta, S. Liao, J. L. Newstead, L. E. Strigari, and J. W. Walker, *Phys. Rev. D* **96**, 095007 (2017), arXiv:1612.06350 [hep-ph].  
[45] P. Coloma, P. B. Denton, M. C. Gonzalez-Garcia, M. Maltoni, and T. Schwetz, *JHEP* **04**, 116 (2017), arXiv:1701.04828 [hep-ph].  
[46] M. Abdullah et al., (2022), arXiv:2203.07361 [hep-ph].  
[47] J. Billard, L. Strigari, and E. Figueroa-Feliciano, *Phys. Rev. D* **89**, 023524 (2014), arXiv:1307.5458 [hep-ph].  
[48] C. A. J. O’Hare, *Phys. Rev. Lett.* **127**, 251802 (2021), arXiv:2109.03116 [hep-ph].  
[49] J. Tang and B.-L. Zhang, *Phys. Rev. D* **108**, 062004 (2023), arXiv:2304.13665 [hep-ph].



- [50] M. W. Goodman and E. Witten, *Phys. Rev. D* **31**, 3059 (1985).
- [51] A. Drukier and L. Stodolsky, *Phys. Rev. D* **30**, 2295 (1984).
- [52] Z. Bo *et al.* (PandaX), (2024), [arXiv:2407.10892 \[hep-ex\]](#).
- [53] E. Aprile *et al.* (XENON), (2024), [arXiv:2408.02877 \[nucl-ex\]](#).
- [54] N. Vinyoles, A. M. Serenelli, F. L. Villante, S. Basu, J. Bergström, M. C. Gonzalez-Garcia, M. Maltoni, C. Peña Garay, and N. Song, *Astrophys. J.* **835**, 202 (2017), [arXiv:1611.09867 \[astro-ph.SR\]](#).
- [55] J. N. Bahcall, E. Lisi, D. E. Alburger, L. De Braeckeleer, S. J. Freedman, and J. Napolitano, *Phys. Rev. C* **54**, 411 (1996), [arXiv:nucl-th/9601044](#).
- [56] J. N. Bahcall, A. M. Serenelli, and S. Basu, *Astrophys. J. Suppl.* **165**, 400 (2006), [arXiv:astro-ph/0511337](#).
- [57] B. Aharmim *et al.* (SNO), *Phys. Rev. C* **88**, 025501 (2013), [arXiv:1109.0763 \[nucl-ex\]](#).
- [58] S. Abe *et al.* (KamLAND), *Phys. Rev. C* **84**, 035804 (2011), [arXiv:1106.0861 \[hep-ex\]](#).
- [59] K. Abe *et al.* (Super-Kamiokande), *Phys. Rev. D* **94**, 052010 (2016), [arXiv:1606.07538 \[hep-ex\]](#).
- [60] M. Agostini *et al.* (Borexino), *Phys. Rev. D* **101**, 062001 (2020), [arXiv:1709.00756 \[hep-ex\]](#).
- [61] R. H. Helm, *Phys. Rev.* **104**, 1466 (1956).
- [62] S. Klein and J. Nystrand, *Phys. Rev. C* **60**, 014903 (1999), [arXiv:hep-ph/9902259](#).
- [63] V. Cirigliano, M. L. Graesser, and G. Ovanessian, *JHEP* **10**, 025 (2012), [arXiv:1205.2695 \[hep-ph\]](#).
- [64] J. Menendez, D. Gazit, and A. Schwenk, *Phys. Rev. D* **86**, 103511 (2012), [arXiv:1208.1094 \[astro-ph.CO\]](#).
- [65] P. Klos, J. Menéndez, D. Gazit, and A. Schwenk, *Phys. Rev. D* **88**, 083516 (2013), [Erratum: *Phys. Rev. D* **89**, 029901 (2014)], [arXiv:1304.7684 \[nucl-th\]](#).
- [66] L. Vietze, P. Klos, J. Menéndez, W. C. Haxton, and A. Schwenk, *Phys. Rev. D* **91**, 043520 (2015), [arXiv:1412.6091 \[nucl-th\]](#).
- [67] M. Hoferichter, P. Klos, and A. Schwenk, *Phys. Lett. B* **746**, 410 (2015), [arXiv:1503.04811 \[hep-ph\]](#).
- [68] A. L. Fitzpatrick, W. Haxton, E. Katz, N. Lubbers, and Y. Xu, *JCAP* **02**, 004 (2013), [arXiv:1203.3542 \[hep-ph\]](#).
- [69] N. Anand, A. L. Fitzpatrick, and W. C. Haxton, *Phys. Rev. C* **89**, 065501 (2014), [arXiv:1308.6288 \[hep-ph\]](#).
- [70] F. Bishara, J. Brod, B. Grinstein, and J. Zupan, *JCAP* **02**, 009 (2017), [arXiv:1611.00368 \[hep-ph\]](#).
- [71] F. Bishara, J. Brod, B. Grinstein, and J. Zupan, *JHEP* **11**, 059 (2017), [arXiv:1707.06998 \[hep-ph\]](#).
- [72] E. E. Jenkins and A. V. Manohar, *Phys. Lett. B* **255**, 558 (1991).
- [73] J. D. Walecka, *Theoretical nuclear and subnuclear physics*, Vol. 16 (1995).
- [74] J. S. O'Connell, T. W. Donnelly, and J. D. Walecka, *Phys. Rev. C* **6**, 719 (1972).
- [75] T. W. Donnelly and R. D. Peccei, *Phys. Rept.* **50**, 1 (1979).
- [76] R. Abdel Khaleq, J. L. Newstead, C. Simenel, and A. E. Stuchbery, (2024), [arXiv:2405.20060 \[hep-ph\]](#).
- [77] K. Scholberg, *Phys. Rev. D* **73**, 033005 (2006), [arXiv:hep-ex/0511042](#).
- [78] S. Davidson, C. Pena-Garay, N. Rius, and A. Santamaria, *JHEP* **03**, 011 (2003), [arXiv:hep-ph/0302093](#).
- [79] E. E. Jenkins, A. V. Manohar, and P. Stoffer, *JHEP* **03**, 016 (2018), [Erratum: *JHEP* **12**, 043 (2023)], [arXiv:1709.04486 \[hep-ph\]](#).
- [80] R. L. Workman *et al.* (Particle Data Group), *PTEP* **2022**, 083C01 (2022).
- [81] W. Haxton and C. Lunardini, *Comput. Phys. Commun.* **179**, 345 (2008), [arXiv:0706.2210 \[nucl-th\]](#).
- [82] D. Akimov *et al.* (COHERENT), (2018), [10.5281/zenodo.1228631](#), [arXiv:1804.09459 \[nucl-ex\]](#).
- [83] G. L. Fogli, E. Lisi, A. Marrone, D. Montanino, and A. Palazzo, *Phys. Rev. D* **66**, 053010 (2002), [arXiv:hep-ph/0206162](#).
- [84] W. Ma *et al.* (PandaX), *Phys. Rev. Lett.* **130**, 021802 (2023), [arXiv:2207.04883 \[hep-ex\]](#).
- [85] T. E. Gonzalo and M. Lucente, *Eur. Phys. J. C* **84**, 119 (2024), [arXiv:2303.15527 \[hep-ph\]](#).
- [86] D. Aristizabal Sierra, N. Mishra, and L. Strigari, (2024), [arXiv:2409.02003 \[hep-ph\]](#).
- [87] D. Akimov *et al.* (COHERENT), *JINST* **17**, P10034 (2022), [arXiv:2111.02477 \[physics.ins-det\]](#).